Nature Environment and Pollution Technology
An International Quarterly Scientific Journal

p-ISSN: 0972-6268
(Print copies up to 2016)
e-ISSN: 2395-3454

Vol. 25 | No. 2 | Article ID B4383 | 2026

Original Research Paper

https://doi.org/10.46488/NEPT.2026.v25i02.B4383

Open Access Journal

# Synthesis of a Novel Activated Carbon/ZnO Nanocomposite from the Dead Bark of Indian Jujube for Efficient Removal of Cationic Dye Pollutant

**Rekha Sharma[1], Bhanupriya Mordhiya[1]†, Parmeshwar Lal Meena[1], Pooja Meena[1] and Surendra Dutt Arya[2]**

[1]Department of Chemistry, University of Rajasthan, Jaipur, Rajasthan, India

[2]Saras Dairy, Jaipur, Rajasthan, India

†Corresponding author: Bhanupriya Mordhiya; bmordhiya@gmail.com

**Abbreviation: Nat. Env. & Poll. Technol.**
**Website: www.neptjournal.com**

*Received:* 01-08-2025
*Revised:* 06-10-2025
*Accepted:* 08-10-2025

*Key Words:*

Activated carbon
ZnO nanocomposite
*Ziziphus mauritiana*
Toluidine blue
Adsorption
Wastewater treatment

*Citation for the Paper:*

Sharma, R., Mordhiya, B., Meena, P.L., Meena, P. and Arya, S.D., 2026. Synthesis of a novel activated carbon/ZnO nanocomposite from the dead bark of Indian Jujube for efficient removal of cationic dye pollutant. *Nature Environment and Pollution Technology*, 25(2), B4383. https://doi.org/10.46488/NEPT.2026.v25i02.B4383

*Note: From 2025, the journal has adopted the use of Article IDs in citations instead of traditional consecutive page numbers. Each article is now given individual page ranges starting from page 1.*



## ABSTRACT

In this study, a novel activated carbon/zinc oxide (AC/ZnO) nanocomposite was synthesized from the dead bark of *Ziziphus mauritiana* (Indian jujube) using chemical activation and high-temperature treatment. The nanocomposite was characterized using FTIR, XRD, BET, FESEM, TEM, XPS, and zeta potential analyses, which confirmed its porous structure and ZnO incorporation. Batch adsorption experiments were conducted to evaluate the ability of the adsorbent to remove toluidine blue (TB) dye from aqueous solutions. Under optimized conditions (0.04 g of adsorbent in 100 mL of dye solution at pH 11.5, a contact time of 50 min, and 25 ± 2°C), the nanocomposite achieved a maximum removal efficiency of 99.6% and an adsorption capacity of 49.9 $mg.g^{-1}$. The adsorption process followed the Langmuir isotherm model and pseudo-second-order kinetics, indicating monolayer chemisorption. The thermodynamic parameters confirmed that the process was spontaneous and endothermic. The nanocomposite retained over 90% efficiency after four regeneration cycles, demonstrating its stability and reusability. These findings highlight the potential of *Z. mauritiana*-derived AC/ZnO as a sustainable and cost-effective adsorbent for removing dyes from wastewater.

## INTRODUCTION

Water contamination by synthetic dyes has become a global environmental challenge owing to their complex aromatic structures, high stability, and resistance to biodegradation (Hansima et al. 2021). Large volumes of colored effluents are released daily from the textile, leather, paper, paint, cosmetics, and pharmaceutical industries, leading to severe ecological and health impacts (Hu et al. 2025, Agrawal et al. 2021, Hambisa et al. 2022). Once discharged into aquatic systems, dyes reduce dissolved oxygen, hinder photosynthesis, and can bioaccumulate through the food chain, posing mutagenic and carcinogenic risks to organisms (Ahmad et al. 2020, Jani et al. 2022, Yadav et al. 2021). Conventional wastewater treatment methods, such as coagulation–flocculation, oxidation, and biological degradation, are either expensive, produce large amounts of sludge, or exhibit limited efficiency in achieving complete dye removal (Khazaal et al. 2022, Nath et al. 2018). Therefore, there is a pressing need for sustainable and efficient adsorbents to address this issue.

Among the various treatment methods, adsorption has emerged as a promising technique because of its simplicity, cost-effectiveness, and high efficiency in removing dyes from water (Akhtar et al. 2025, Feng et al. 2020). Activated carbon (AC) remains the most widely used adsorbent because of its large surface area, tunable porosity, and active surface functionalities (Ahmad et al. 2015, Luo et al. 2019). However, the commercial production of AC relies on non-renewable precursors and incurs high costs, restricting its large-scale application (Abo El Naga et al. 2019, Tripathi et al. 2013). To overcome this limitation, researchers have explored low-

cost and renewable precursors, such as agricultural residues, fruit peels, seeds, and industrial by-products (Shrivastva et al. 2022, Deshmukh et al. 2022, Gupta et al. 2025). Hybrid nanocomposites, in which AC is combined with metal oxides (e.g., ZnO, $TiO_2$, and $MnO_2$), have attracted attention because of their enhanced surface activity, stability, and adsorption capacity (Nguyen et al. 2020, Mordhiya et al. 2024).

Despite these advances, the specific utilization of woody biomass and bark-based residues remains largely unexplored. Most studies have focused on seeds, cores, or shells (Bouchelkia et al. 2023, Malika et al. 2021, Venkatesan et al. 2024), while dead bark materials are often discarded as waste despite being lignocellulose-rich precursors suitable for producing high-quality activated carbon. To the best of our knowledge, no prior reports exist on the synthesis of AC/ZnO nanocomposites using *Ziziphus mauritiana* (Indian jujube) bark. This represents a significant research gap because Z. mauritiana is widely available in Rajasthan and other semi-arid regions of India, and its bark is usually left unused. Valorizing such biomass not only reduces the environmental burden but also provides a low-cost route for preparing efficient nanocomposites.

The novelty of the present study lies in addressing this research gap by developing, for the first time, an AC/ZnO nanocomposite derived from Z. Mauritiana bark. Although AC/ZnO systems have been reported for other plant residues, this precursor choice has not been investigated. Therefore, our approach combines sustainable waste valorization with the design of efficient adsorbents for dye remediation.

This study focuses on synthesizing an AC/ZnO nanocomposite from Z. mauritiana bark and systematically investigating its efficiency in removing cationic dye pollutants from aqueous solutions, using toluidine blue (TB) as a model contaminant. A comprehensive suite of characterizations was employed, including FTIR, XRD, FESEM, TEM, BET, XPS, and zeta potential analysis, to confirm the nanocomposite structure, morphology, and surface properties. Batch adsorption experiments were performed to evaluate the effects of pH, adsorbent dosage, initial dye concentration, contact time, and temperature. Adsorption isotherms (Langmuir, Freundlich, Temkin, and Dubinin–Radushkevich), kinetics (pseudo-first-order, pseudo-second-order, Elovich, and intraparticle diffusion models), and thermodynamics were studied to elucidate the adsorption mechanism. The recyclability was tested over four cycles to examine the reusability.

Three contributions reinforce the novelty and relevance of this study.

**Sustainability:** Utilization of waste biomass (Z. mauritiana bark) to produce a high-quality AC/ZnO nanocomposite.

**Performance:** Near-complete dye removal (99.6% under optimized conditions) was achieved, with an adsorption capacity comparable to or better than that of reported biomass-based nanocomposites.

**Future Feasibility:** Demonstration of recyclability and acknowledgment of limitations (e.g., Zn-leaching and multi-pollutant systems) that pave the way for future investigations.

In summary, this study introduces a novel biomass precursor for AC/ZnO nanocomposites and establishes the adsorption potential of the synthesized material under optimized laboratory conditions.

## MATERIALS AND METHODS

### Chemicals Used

The materials used in this study included zinc chloride ($ZnCl_2$), hydrochloric acid (HCl), sodium hydroxide (NaOH), distilled water, and toluidine blue (TB) dye ($C_{15}H_{14}N_3ClS$). The primary raw material employed was the dead bark of the native Indian jujube. All chemicals used were of analytical grade. Toluidine blue, a heterocyclic synthetic organic dye, was used as a model contaminant to simulate water pollution. With a molecular weight of 319.85 $g.moL^{-1}$, TB is highly water-soluble and remains stable for long durations under standard temperature and pressure conditions. Due to its poisonous, carcinogenic, and non-biodegradable nature, it is a chemical that should be avoided at all costs.

### Preparation of Nanoadsorbent

Naturally dried bark of the *Ziziphus mauritiana* (Indian jujube) shrub was obtained locally. It was essential to eliminate any dust or pollutants that had stuck to the bark of the Indian jujube. The bark was initially chopped into small fragments and meticulously washed with tap water to remove surface contaminants, followed by a rinse with distilled water. The material was carbonized by heating in a furnace at 500°C for 2 h. Upon cooling, the resultant black residue was pulverized into a fine powder (Sulaiman et al. 2021). To synthesize the AC/ZnO nanocomposite, one gram of *Ziziphus mauritiana* charcoal was combined with one gram of zinc chloride, and a few drops of water were incorporated to achieve a suitable paste consistency. The paste was desiccated in an oven at 80°C for 24 h. The dry paste was subsequently heated in a muffle furnace at 500°C for 1 h. Following cooling, the samples were washed multiple times with distilled water and finally rinsed with ethanol. The samples were subsequently dehydrated in an oven at 85°C for 3 h (Fig. 1). The AC/ZnO nanocomposite was stored in an airtight container for subsequent characterization and used to examine the adsorption behavior of the TB dye

from aqueous solutions under various experimental conditions.

### Batch Equilibrium Investigation

The effects of several parameters, including pH, contact time, dye concentration, and adsorbent dose, on the adsorption effectiveness of the nanoadsorbent were examined using a series of batch equilibrium tests. TB dye was used as a stock solution for the experiments, which were conducted at room temperature. Dye solutions with concentrations ranging from 10 to 60 mg.$L^{-1}$ were prepared by diluting the stock solution. To maintain appropriate pH levels, diluted solutions of NaOH and HCl were used to adjust the solutions to pH values of 4, 8, 10, and 11.5, respectively. 20-50 mg was used. The adsorption kinetics, isotherms, and thermodynamic factors were studied to gain a more profound understanding of the adsorption mechanism. The solution was constantly stirred throughout each experiment, and once the required amount of time had passed, the mixture was centrifuged and filtered through a Whatman filter paper. UV-Vis spectrophotometry was used to measure the dye concentration. The equilibrium adsorption capacity ($q_e$), dye removal efficiency, and adsorption capacity ($q_t$) at various process phases were calculated using the standard equations.

### Instrumentation

The objectives of clarifying the morphology and structure of nanoadsorbents and confirming the adsorption of dye from an aqueous solution were achieved by employing various spectroscopic techniques. The crystalline structure of the nanoadsorbents was investigated using XRD. The produced nanoadsorbent was subjected to XRD analysis using a PANalytical X'Pert PRO diffractometer operating at 40 mA and 40 kV with Cu Kα radiation (λ = 1.5406 Å). To quantify the particle size and evaluate the quality of the crystalline phase, the diffraction pattern was recorded over a 2θ range of 10° to 80°. Furthermore, a Perkin Elmer FTIR spectrometer operating in transmission mode was used to perform FTIR spectroscopy in the range of 4000–400 $cm^{-1}$. The objectives of this analysis were to identify the functional groups on the adsorbent surface and observe any changes in bonding properties following dye adsorption (TEM, FEI CM12). A field-emission scanning electron microscope (FESEM, Nova Nano FESEM-450 (FEI)) was used to obtain TEM and FESEM images, respectively. These images were captured to assess the microstructural and textural characteristics of adsorbents. BET analysis was performed using a surface analyzer (NOVAtouch 2LX) to determine the specific surface area, pore size, and pore distribution of the material. EDS was used to confirm the elemental composition of the synthesized nanocomposite. The UV-Vis absorbance of the dye solutions and adsorbent was measured using a Shimadzu UV-2600 UV-vis spectrophotometer.

## RESULTS AND DISCUSSION

### Characterization of Nanoadsorbent

#### *XRD-Based Structural Analysis*

Fig. 2 presents the XRD patterns for both pure ZnO and

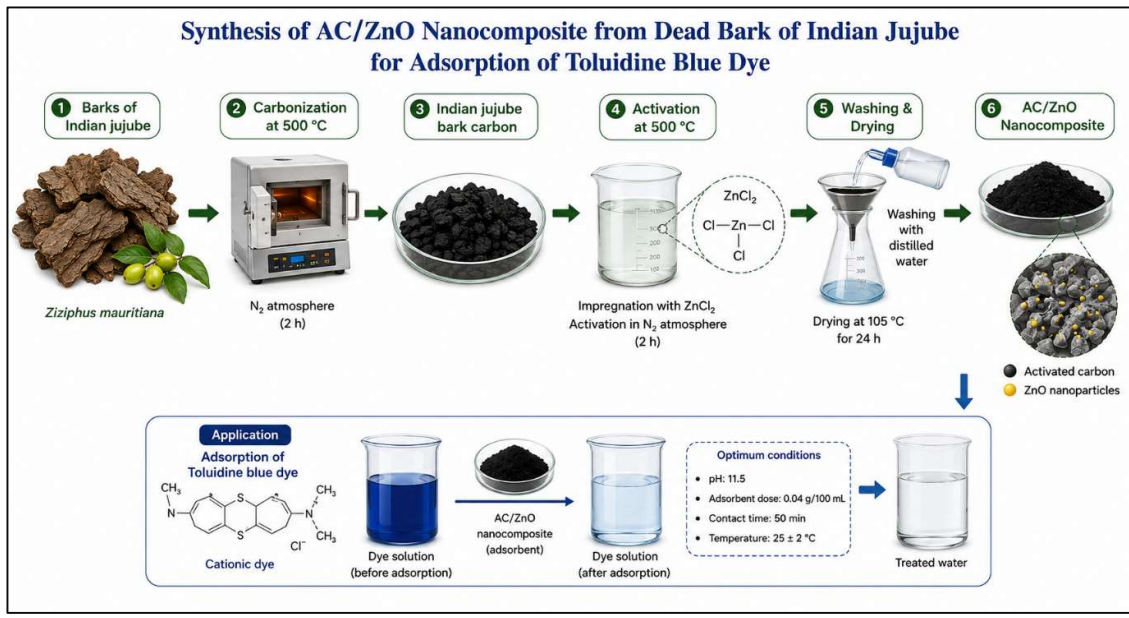


Fig. 1: Schematic depiction of the pathway for the AC/ZnO nanocomposite derived from Indian jujube dead bark.

the AC/ZnO nanocomposite. The diffraction peaks of pure ZnO appeared at 2θ values of 31.90°, 34.58°, 36.52°, 47.70°, 56.75°, 62.96°, 66.51°, 68.28°, 69.17°, 72.53°, and 77.15°, which correspond to the (100), (002), (101), (102), (110), (103), (200), (112), (201), (202), (004), and (202) planes of the hexagonal wurtzite ZnO crystal structure. In the case of the AC/ZnO composite, diffraction peaks were observed at 31.78°, 34.48°, 36.26°, 47.56°, 56.59°, 62.81°, 66.32°, 67.73°, 69.14°, 72.66°, and 77.11°, corresponding to the same crystal planes of the hexagonal wurtzite ZnO structure. Additionally, the peaks at 2θ values of 26.65° and 44.72° are attributed to the (002) and (100) reflection planes of the hexagonal graphite structure present in AC. (Ghaedi et al. 2012).

On mixing ZnO with activated carbon, the XRD peak positions related to ZnO in the composite shifted toward slightly lower 2θ values compared to pure ZnO, revealing the mixing of ZnO nanospheres with activated nanocarbon sheets. The Debye–Scherrer relation was used to estimate the particle size of the AC. This was accomplished by considering the diffraction peak, which had a value of 2θ = 36.26°, λ = 1.5406 Å, and the full width at half maximum (FWHM) (β) of the peak. The average particle size of the produced AC/ZnO nanocomposition was 61.72 nm.

### *FTIR Analysis*

Fig. 3 shows the FTIR spectra of the AC/ZnO nanocomposite. The peak observed at 1331 $cm^{-1}$ corresponds to the stretching vibrations of the C–C bonds found in the activated carbon (Abdel-Ghani et al. 2019). The peak at 1508 $cm^{-1}$ indicates the presence of an aromatic ring in the adsorbent. The peak at 1696 $cm^{-1}$ is attributed to the stretching vibration of carbonyl (C=O) groups, while the 1777 $cm^{-1}$ peak is associated with ester linkages in the nanoadsorbent (Abo El Naga et al.

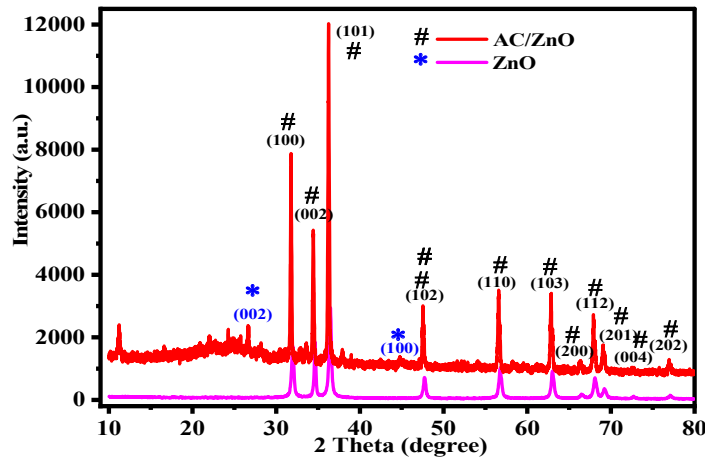


Fig. 2: XRD pattern of the pure ZnO and AC/ZnO nanocomposite.

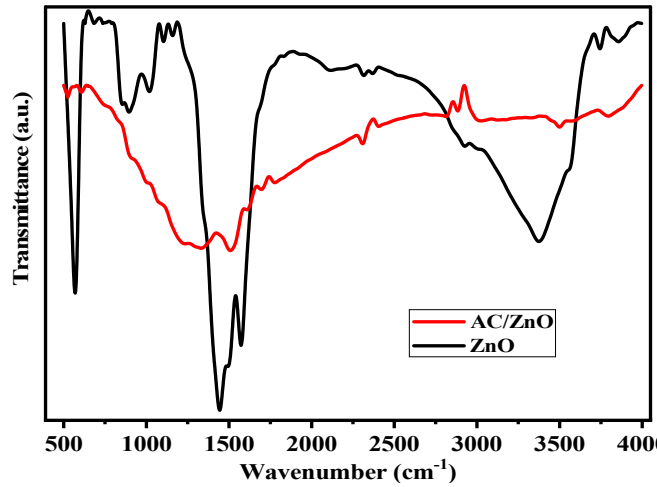


Fig. 3: FTIR spectra of the pure ZnO and AC/ZnO nanoadsorbent.

2019). Bending vibrations of C–H bonds were responsible for the peaks at 2308 $cm^{-1}$, 2813 $cm^{-1}$, and 2884 $cm^{-1}$ (Omri & Benzina 2012). A peak at 525 $cm^{-1}$ corresponds to the stretching vibration of the Zn–O bond, whereas pure ZnO typically shows this vibration at 570 $cm^{-1}$. The shift to a lower wavenumber upon incorporation of activated carbon confirms the successful integration of ZnO nanospheres into the AC nanosheets. After the dye was adsorbed onto the nanoadsorbent surface, changes in the FTIR spectrum were observed (Fig. 3). A broad peak at 3314 $cm^{-1}$ confirms the presence of alcohol groups due to the O–H stretching vibrations.

### Images from the FESEM and HRTEM

The presence of various elements and their distribution along the surface of the nanoadsorbent is visible in the FESEM images.

Fig. 4 presents the morphological analysis of the AC/ZnO nanocomposite, as observed through field-emission scanning electron microscopy (FESEM). After some time, FESEM images showed hollow chambers surrounding the nanoadsorbent. The primary locations for adsorbing contaminants from water and removing them are these hollow chambers. As these empty areas become occupied, the nanoadsorbents move closer to peak saturation. The FESEM images provide evidence that these contaminants eventually precipitate in the hollow chambers in which they are contained. Sticky polar interactions occur within the hollow chambers surrounding the nanocomposite. These sticky polar interactions facilitate the chelation of hazardous contaminants in the water phase, which are responsible for binding pollutants. Through polar-polar interactions, the AC/ZnO nanocomposite enables the selective removal of

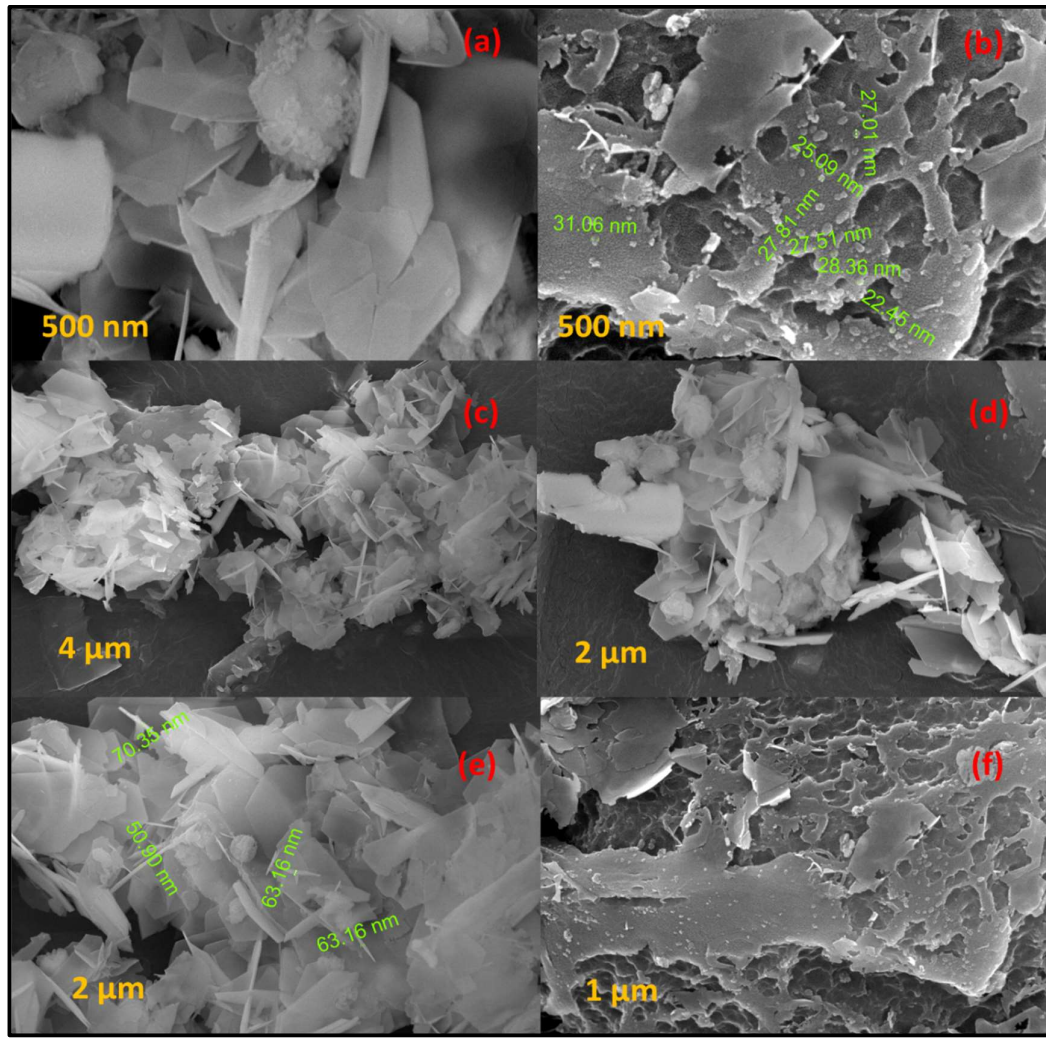


Fig. 4: FESEM images of AC/ZnO nanocomposite.

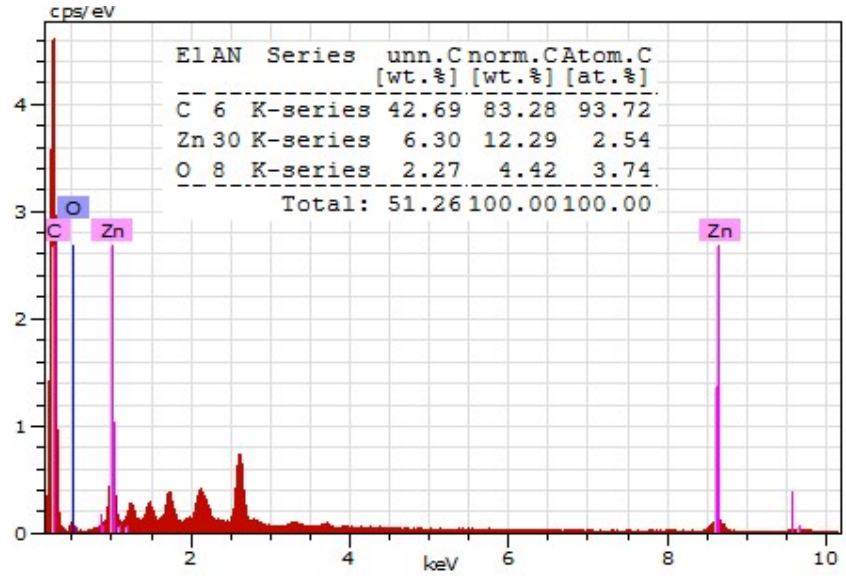


Fig. 5: EDS image of AC/ZnO nanocomposite.

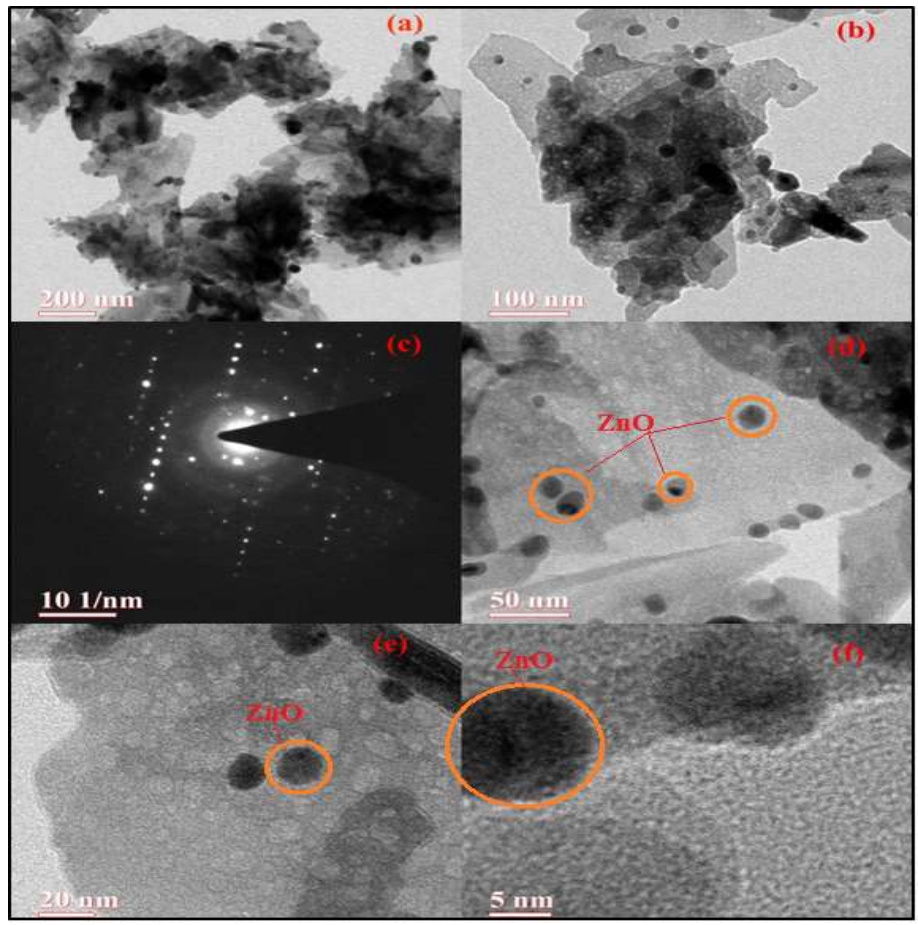


Fig. 6: HRTEM images of AC/ZnO nanocomposite.

contaminants from water. Owing to the unequal distribution of hollow chambers around the nanoadsorbent, it may be concluded that the AC/ZnO nanocomposite is amorphous in its natural state (Elmaguana et al. 2020). Fig. 5 displays the EDS spectrum of the AC/ZnO nanocomposite adsorbent, showing distinct peaks corresponding to Zn, O, and C. The respective weights and atomic percentages are provided in the inset table of the figure. Fig. 6 shows the TEM and HRTEM images of the synthesized AC/ZnO composite, revealing that the ZnO nanostructures have a spherical shape and are distributed across the surface of the activated carbon nanosheets. The selected area electron diffraction (SAED) pattern of the composite, shown in Fig. 6(c), features bright diffraction spots.

**Photoelectron Emission Spectra (XPS) Analysis**

To obtain more information about the prepared AC/ZnO nanocomposite from the bark of Indian jujube, XPS spectral analysis was performed, as shown in Fig. 7.

Fig.7 (a) shows the survey spectrum of the AC/ZnO nanocomposite, which contains peaks related to Zn, O, and C. The peak observed at 279.50 eV in Fig. 7(b) represents C1s and confirms the existence of carbon in the +1 oxidation state. Other peaks in the deconvoluted XPS spectra are reported at 280.94 and 284.73 eV, corresponding to C-O and C-C bonding, respectively. The peak at 528.90 eV in Fig. 7(c) indicates the presence of the O1s state, and other peaks observed in the deconvoluted spectrum are reported at binding energy values of 527.13 and 525.81 eV. The XPS peaks corresponding to the binding energy values of 1018.21 eV and 1041.45 eV, which can be attributed to Zn2p3/2 and Zn2p1/2, respectively, are shown in Fig. 7(d). The difference in the binding energy values between the Zn2p3/2 and Zn2p1/2 peaks was ~23 eV, indicating the existence of the $Zn^{2+}$ state of Zn in the lattice.

**Analysis of Zeta Potential Characteristics**

The zeta potential is a key parameter used to assess the stability of nanomaterials. Nanoparticles with highly positive or negative zeta potential values tend to repel each other more strongly, which helps prevent aggregation and allows them to redisperse easily in a medium. Typically, a zeta potential of at least ±30 mV is considered necessary for effective electrostatic and steric stabilization (Lunardi et al. 2020). The AC/ZnO nanocomposite synthesized using the bark of Indian jujube exhibited a zeta potential of +10 mV, suggesting limited stability and moderate dispersibility (Fig. 8).

***BET Analysis***

BET analysis was employed to estimate the pore size, pore

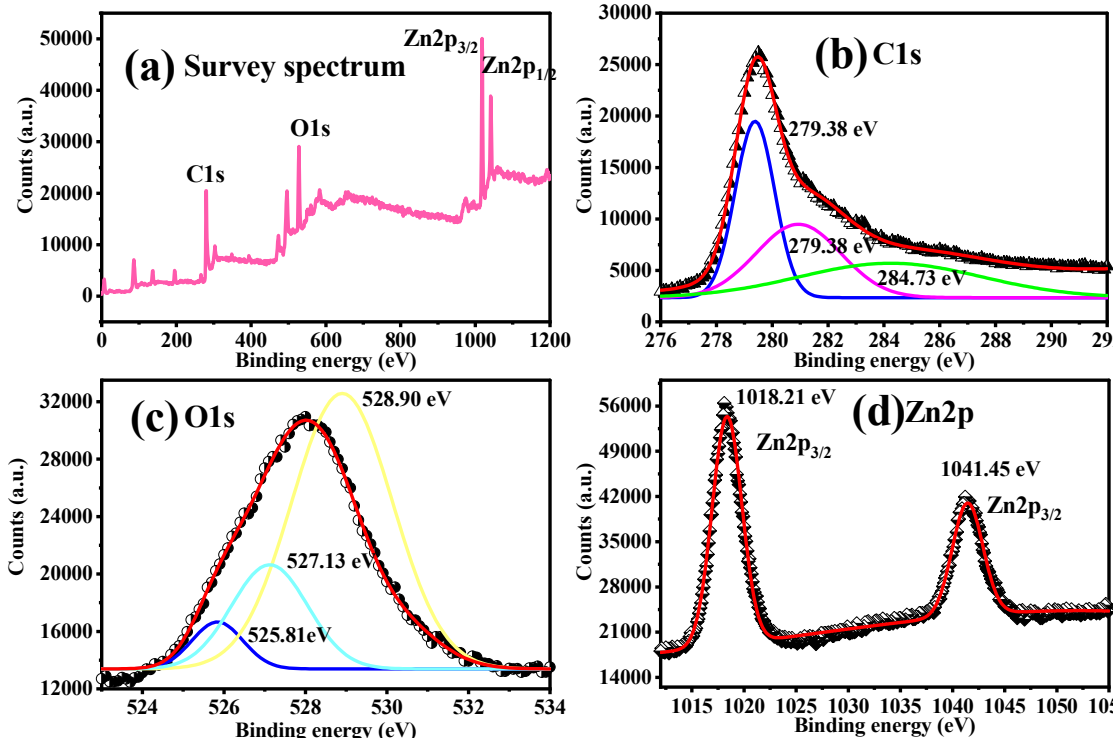


Fig. 7: XPS spectra of AC/ZnO nanocomposite.

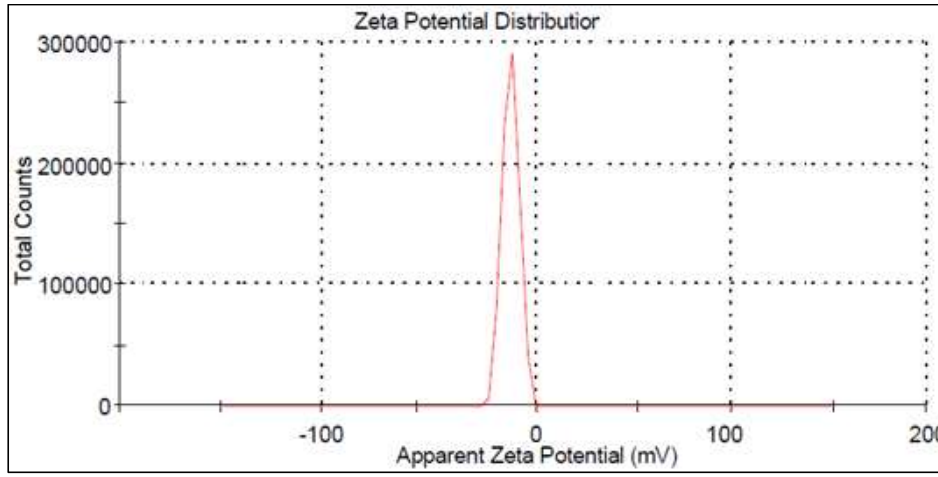


Fig. 8: Zeta potential of the prepared AC/ZnO nanocomposite of Indian Jujube.

volume, and surface area of the synthesized nanoadsorbent. Fig. 9(a) shows the nitrogen ($N_2$) sorption isotherm of the nanoadsorbent, which corresponds to a Type IV isotherm. The creation of a monolayer is represented by a flat region in the middle. When the pressure was extremely low, the microspores began to fill with nitrogen gas. At the knee, monolayers are created, and at medium pressure, multilayers are formed. Capillary condensation occurred at higher pressures. When the $P/P_0$ ratio increased, a greater volume of gas was adsorbed, indicating that the nanoadsorbent possessed a mesoporous crystal structure (Abdel-Ghani et al. 2019). The surface area of the nanoadsorbent was calculated to be 323.997 $m^2.g^{-1}$. The BJH approach, which utilizes the Kelvin equation to establish a correlation between pore diameter and pore condensation pressure, was employed to calculate the pore size distribution (Fig. 9 (d)). Using this

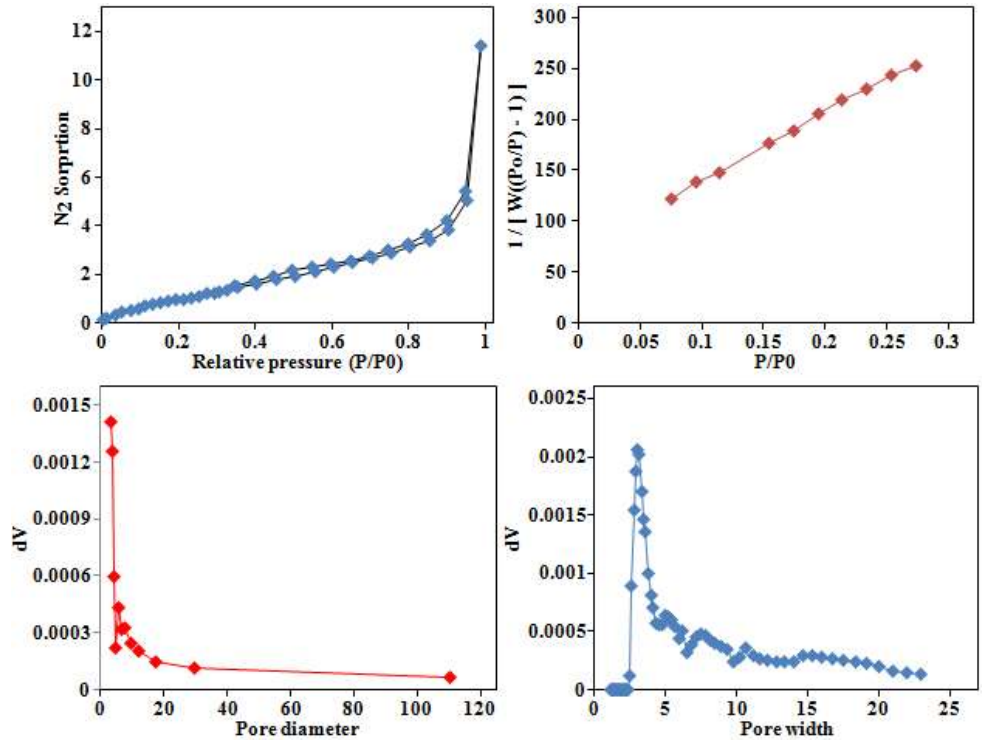


Fig. 9: (a) Nitrogen sorption isotherm, (b) BET adsorption isotherm, and BJH pore size distribution curve(c) and (d) of AC/ZnO-nanocomposite synthesized from Indian jujube dead bark.

equation, the average pore volume and average pore diameter were determined to be 0.255 cc.g$^{-1}$ and 3.15 nm, respectively.

## Adsorption Parameters

### *Contact Time Impact*

The fluctuation in the adsorption of toluidine dye from the aqueous phase by the nanoadsorbent is depicted in Fig. 10, illustrating variations in the contact time. Within the first 30 min, the adsorption process occurred rapidly. After 60 min, the adsorption rate was equal to the desorption rate. The manufactured nanoadsorbent selectively adsorbed the toluidine blue dye from the aqueous phase. To conduct the adsorption investigation, the time parameter was varied from 10 to 60 min. A representation of the adsorption investigation is shown in Fig. 10. At an earlier stage, there was a significant acceleration in the adsorption process because the adsorption sites of the nanocomposite that were open for adsorption were not yet occupied. As the vacant sites on the AC-ZnO nanocomposite became occupied by various molecules, the adsorption rate reached equilibrium with the desorption rate (Naranjo et al. 2023). An equilibrium state was reached after 50 min of contact time. Thus, the optimal contact duration for the adsorption investigation was 50 min. Because the sorption sites are filled with adsorbate molecules, the adsorption performance does not change after the equilibrium of the adsorption process is reached. Furthermore, when the contact length was increased from 50 to 60 min, no discernible difference in adsorption capability was observed. This was because the adsorbing spots on the nanocomposite surface were saturated.

### *Initial Dye Concentration Impact*

An investigation was conducted to examine the effect of varying TB dye concentrations on the adsorption process, and the results are presented in Fig. 11(a). The dye concentration was varied from 10 mg.L$^{-1}$ to 70 mg.L$^{-1}$, while maintaining a constant adsorbent dosage of 0.02 g throughout the experiment. The research was conducted at a steady pH of 11.5. According to the calculations, the percentage of TB dye removed decreased from 99.63% to 37.63%. Consequently, the dose level of the AC/ZnO nanocomposite was maintained. At lower dye concentrations, the surface-active sites of the nanocomposite are less occupied (González-García 2018). Consequently, there is a greater availability of surface-active sites, which increases the frequency of adsorption. The adsorption rate decreased when the accessibility of the active sites on the surface was lower, which occurred at higher dye concentrations (A'yuni et al. 2024).

### *Effect of Adsorbent Dose*

A more in-depth explanation of how the quantity of adsorbent affects the removal of dye from the aqueous phase (Weber & Morris 1963) is provided in Fig. 11 (b). When the dose of the AC/ZnO nanocomposite was increased from 0.02 to 0.04 g, the percentage of TB dye removed from the solution increased from 86.08% to 99.60%. However, beyond 0.04 g, the adsorption capacity remained stable. This suggests that adsorption was nearly complete with 0.04 g of the adsorbent and may have been caused by the saturation of empty spaces or the aggregation/agglomeration of adsorbent particles with one another. For further research, 0.02 g of the adsorbent was selected. Increasing the adsorbent dose enhances the surface area and number of adsorption sites while maintaining a consistent dye solution volume and concentration, which may result in improved removal efficiency.

### *pH Impact*

The pH of the dye solution was adjusted within the range of 4–11.5 to investigate its effect on the adsorption of TB onto the AC-ZnO nanocomposite (González-García 2018). The

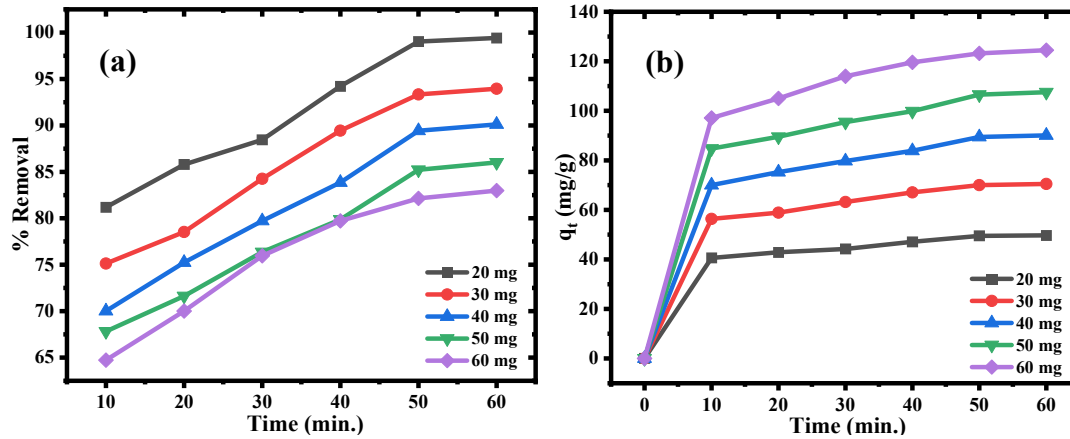


Fig. 10: Effect of contact time on the percentage removal efficiency of TB dye by the AC/ZnO nanocomposite.

results are shown in Fig. 11(c), which illustrates the changes in the adsorption rates. Based on the data presented in Fig. 11(c), it has been determined that the performance of the nanoadsorbent has improved from 74.01% to 99.33%.

### *Temperature Impact*

The adsorption efficiency of the AC/ZnO nanocomposite for the TB dye increased from 99.19% to 99.86% when the temperature of the dye solution was raised to 45°C. Furthermore, as illustrated in Fig. 11(d), the equilibrium adsorption capacity increased from 49.59 $mg.g^{-1}$ to 49.93 $mg.g^{-1}$. This improvement is explained by the fact that higher temperatures cause the viscosity of the dye solution to decrease, allowing the dye to diffuse more quickly. Additionally, as the temperature increased, the dye's intraparticle diffusion rate also increased, thereby enhancing adsorption (Trivedi et al. 2023). The adsorption process is endothermic if the dye removal rate increases with increasing temperature.

## Kinetics Study

A kinetic study was conducted to explore the mechanism of TB dye adsorption onto the nanoadsorbent surface from a research perspective. To analyze the adsorption kinetics and underlying mechanism, several kinetic models were applied, including the pseudo-first-order (PFO) (Neme et al. 2022), pseudo-second-order (PSO) (Al-Harby 2021), Elovich (Al-Harby, 2021), and intra-particle diffusion (IPD) models (Sutherland et. al. 2025). The Elovich model is based on the concept that the solid surface exhibits heterogeneous energy and that the adsorption process becomes slower as more solute is adsorbed (Al-Harby 2021). In the Elovich kinetic model, the initial adsorption rate is denoted by β (g $mg^{-1}.min^{-1}$), and the desorption constant is denoted by α ($mg.g^{-1}.min^{-1}$). To compute the values of β and α, the slope and intercept of the curve produced between $q_e$ and ln t can be employed. The intra-particle diffusion model (IPD) was described by Weber and Morris (Sutherland et. al. 2025) and was employed to identify the rate-determining steps.

The constant C ($mg.g^{-1}$) represents the thickness of the boundary layer, while $k_{id}$ ($mg.g^{-1}\ min^{-1/2}$) is the rate constant for the intraparticle diffusion (IPD) kinetic model. By plotting $q_t$ against $t^{0.5}$, the slope and intercept of the resulting graph provide the values of $k_{id}$ and C, as well as the coefficient of determination. If the IPD plot

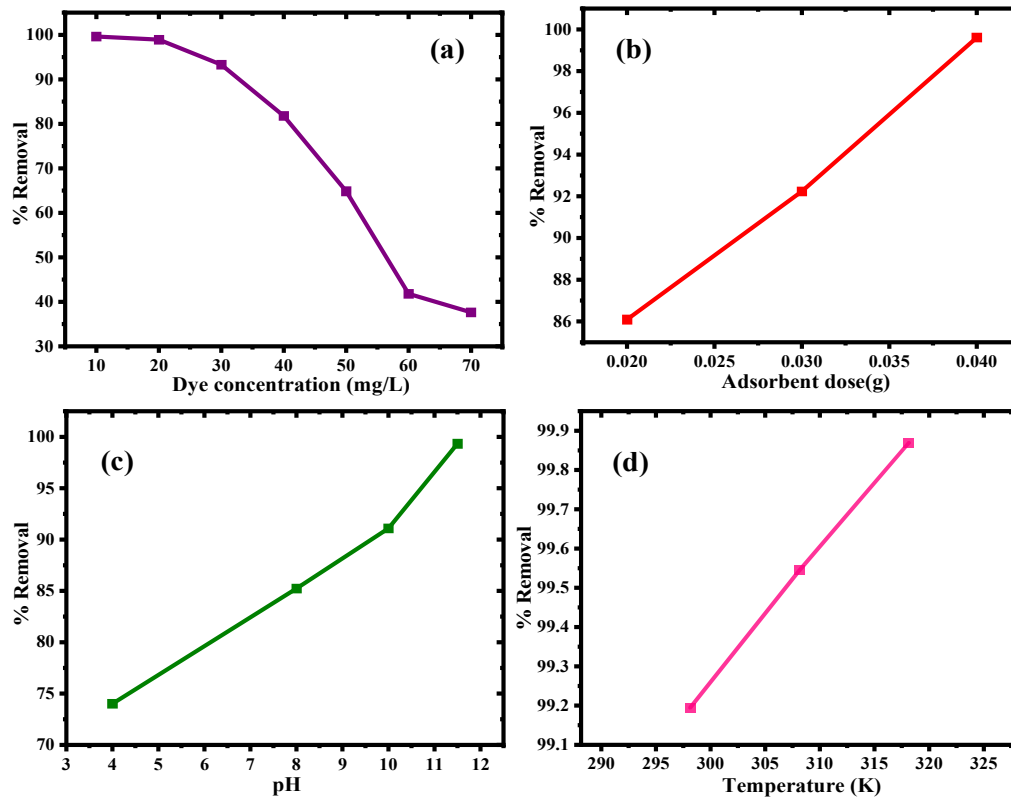


Fig. 11: Effect of (a) initial dye concentration, (b) nanoadsorbent dose, (c) pH, and (d) temperature on the percentage removal efficiency of TB dye by AC/ZnO nanocomposite.

($q_t$ vs. $t^{0.5}$) yields a straight line passing through the origin with no intercept, it indicates that intra-particle diffusion is the sole rate-controlling step in the adsorption process. Fig. 12 presents the kinetic plots for the PFO, PSO, Elovich, and IPD models related to the adsorption of TB dye onto the AC/ZnO nanocomposite synthesized from the bark of Indian jujube. Table 1 summarizes the kinetic parameters of the four models. The suitability of these models was evaluated using two key factors: the regression coefficient ($R^2$) and the closeness between the experimental adsorption capacity ($q_e$, exp) and the calculated one ($q_e$, cal).

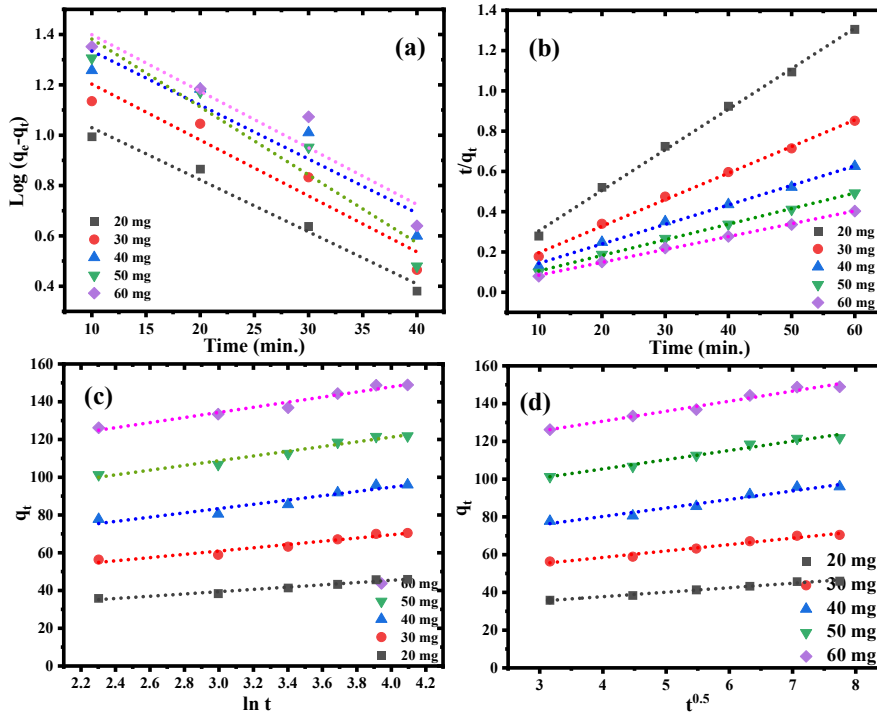


Fig. 12: Depicting (a) pseudo-first order, (b) pseudo-second order, (c) Elovich, and (d) intraparticle diffusion kinetics for TB dye adsorption by the AC/ZnO nanocomposite.

Table 1: Kinetic characteristics of the AC/ZnO nanocomposite for TB dye adsorption.

| Kinetics Models | Parameters | Dye Concentration | | | | |
|---|---|---|---|---|---|---|
| | | 20 mg | 30 mg | 40 mg | 50 mg | 60 mg |
| First order | $q_e$, exp [mg.g$^{-1}$] | 17.206 | 26.67 | 35.463 | 44.951 | 42.161 |
| | $K_1$ [min$^{-1}$] | 0.0476 | 0.0512 | 0.0494 | 0.0622 | 0.05184 |
| | $q_e$, cal [mg.g$^{-1}$] | 49.514 | 70 | 89.433 | 106.53 | 123.22 |
| | R | 0.99 | 0.963 | 0.942 | 0.962 | 0.955 |
| Second order | $q_e$, cal [mg.g$^{-1}$] | 49.652 | 75.816 | 103.306 | 129.032 | 156.495 |
| | $K_2$ [g.mg$^{-1}$.min$^{-1}$] | 0.004 | 0.003 | 0.002 | 0.002 | 0.002 |
| | R | 0.999 | 0.999 | 0.999 | 0.999 | 0.999 |
| Elovich | B | 0.165 | 0.116 | 0.088 | 0.079 | 0.074 |
| | A | 204.96 | 503.83 | 875.62 | 3659.31 | 13950.92 |
| | R | 0.986 | 0.974 | 0.962 | 0.985 | 0.981 |
| Intraparticle | $K_{id}$ | 2.368 | 3.406 | 4.509 | 4.897 | 5.303 |
| | C | 28.253 | 44.887 | 62.174 | 85.792 | 109.47 |
| | R | 0.993 | 0.988 | 0.988 | 0.988S | 0.988 |

Among the models, both the PFO and PSO exhibited $R^2$ values close to unity, indicating a good fit. However, the PSO model showed a better correlation, with $R^2$ values even closer to 1 and a stronger agreement between $q_e$, exp and $q_e$, cal across all TB dye concentrations tested. This suggests that the PSO kinetic model provides a more accurate representation of the adsorption behavior of the TB dye on the AC/ZnO nanocomposite. It is also more effective in predicting parameters related to the adsorbate mass, surface diffusion, and activation/deactivation energies. In addition, the Elovich model provided a reasonable fit to the experimental data, indicating that chemisorption plays a role in the adsorption process. The higher values of α compared to β in the Elovich model further support the observation that adsorption is more favorable than desorption in this system.

Moreover, the presence of nonzero intercepts in the IPD model plots, along with $R^2$ values significantly lower than unity, suggests that intraparticle diffusion is likely not the primary rate-controlling step in the adsorption process (Sutherland et. al. 2025). Consequently, the $R^2$ values deviated from unity.

**Adsorption Equilibrium Studies**

Adsorption equilibrium studies are crucial for removing dyes from aqueous solutions using nano-adsorbents. These studies were used to gain knowledge of the interactions between the dye molecules and the nanoadsorbent composition. Adsorption equilibrium studies often involve the use of adsorption isotherms to describe the relationship between the amount of dye adsorbed onto the nanoadsorbent before equilibrium and the concentration of the remaining dye in the wastewater. One of the assumptions made by the Langmuir isotherm model is that monolayer adsorption occurs on a surface that is homogeneous and has a finite number of similar adsorption sites with the same energy (Sangon et al. 2020). The Langmuir equation can be utilized to predict the adsorption capacity of the nanoadsorbent as well as the equilibrium constant associated with the adsorption energy. The separation factor ($R_L$) can be used to determine whether the adsorption process is beneficial. When $R_L$ is greater than 1, the process is known to be unfavorable; when $R_L$ is equal to 1, the process is considered to be linearly favorable; when $R_L$ is between 0 and 1, the process is supposed to be advantageous, and when $R_L$ is equal to zero, the process is considered to be irreversible.

The Freundlich isotherm model (Neme et al. 2022) is an empirical approach used to describe multilayer adsorption on heterogeneous surfaces (Sajjadi &Goharshadi 2017). According to this hypothesis, the adsorption energy is likely to decrease as the surface coverage increases. The adsorption capacity and intensity of the nanoadsorbent were evaluated using the Freundlich equation, which characterizes the adsorption process using key parameters, including the equilibrium concentration of the dye in the solution ($C_e$) and the amount of dye adsorbed on the nanoadsorbent at equilibrium ($q_e$). The Temkin isotherm is based on the relationship between the coverage of the adsorbent surface by the adsorbate and the heat released during the adsorption process. The isotherm indicates that as the surface of the adsorbent is covered, the heat of sorption decreases.

The Dubinin-Radushkevich adsorption isotherm helps determine the type of adsorption, whether physisorption or chemisorption, and calculates the adsorption energy. In adsorption equilibrium investigations, the correlation coefficients ($R^2$ values) generated by fitting experimental data to the various isotherm models were utilized to determine the degree to which these models accurately described the real behavior of adsorption (Fig. 13). Higher $R^2$ values suggest that the model is a better fit for the experimental data. By conducting adsorption equilibrium studies using nano-adsorbents and analyzing the data using different isotherm models, researchers can gain insights into the adsorption mechanisms, capacity, and effectiveness of nano-adsorbents in removing dyes from wastewater. The linear equations and respective constants obtained for each model are presented in Table 2. Based on the $R^2$ values and isotherm constants, the Langmuir model best fits the experimental data, indicating a monolayer adsorption process. The Freundlich and D-R models also showed strong applicability, suggesting surface heterogeneity. Although the Temkin model contributed additional understanding of the adsorption energy and interactions, its lower $R^2$ values suggest limited suitability for this system.

**Thermodynamic Study of Adsorption**

To gain a better understanding of the practicability and effectiveness of the process, it is essential to study the thermodynamics of adsorption for removing colors from aqueous solutions using nano-adsorbents. The following parameters can be used to determine the spontaneity of adsorption on the surface of nanoadsorbents. Gibbs free energy (Al-Kadhi 2019), enthalpy (Badran & Khalaf 2020), and entropy. Since the adsorption is spontaneous, $\Delta G^{\circ}<0$, adsorption, on the other hand, is not a spontaneous process. A positive $\Delta S$ °indicates increased disorder (Mahvelati-Shamsabadi et al. 2018). When $\Delta S^{\circ}$ is negative, it indicates a reduction in disorder.

Based on the plot of ln $K_c$ versus 1/T depicted in Fig. 14, the slope and intercept were employed to determine the $\Delta H^{\circ}$ and $\Delta S^{\circ}$ values, respectively. A detailed summary

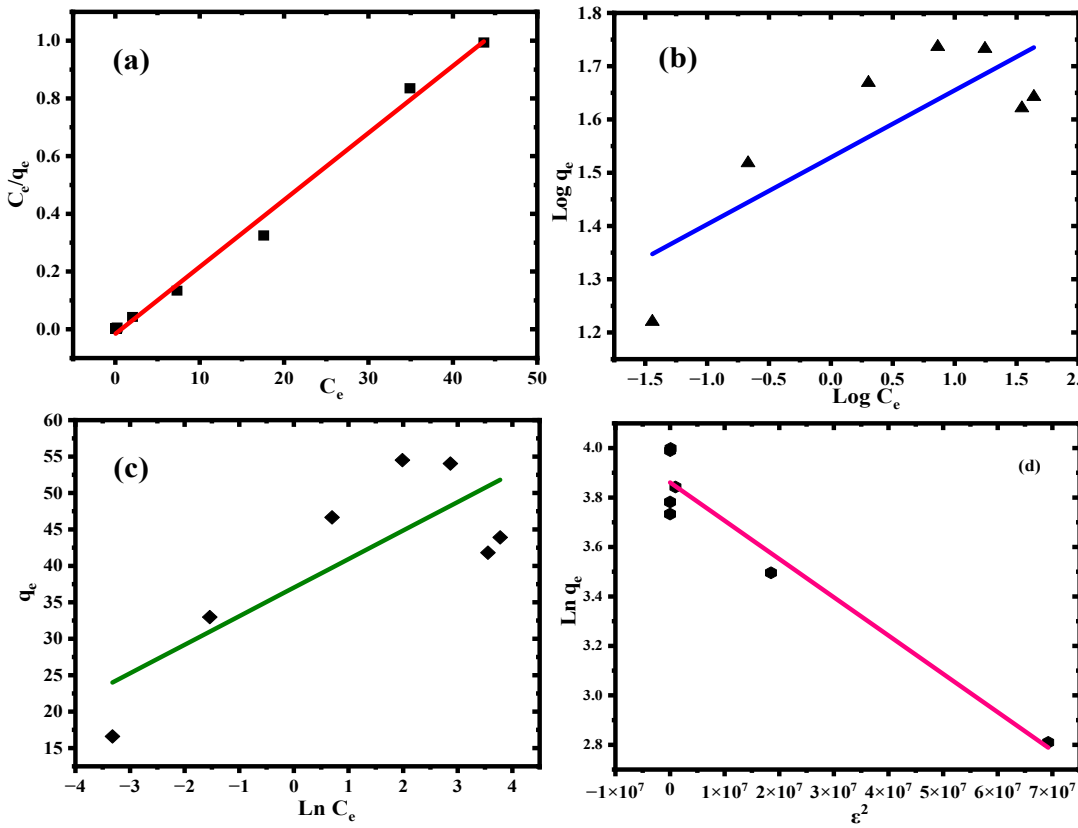


Fig. 13: (a) Langmuir isotherm, (b) Freundlich isotherm, (c) Temkin isotherm, and (d) Dubinin–Radushkevich isotherm plots representing the adsorption of TB dye onto the synthesized AC/ZnO nanocomposite.

Table 2: Isotherm parameters for TB dye removal using the AC/ZnO nanocomposite.

| Isotherms | Paramerers | Values of isotherm parameters |
|---|---|---|
| Langmuir | $q_{max}$ [mg.g$^{-1}$] | 84.034 |
| | $b_L$ [L.mg$^{-1}$] | 8.207 |
| | $R_L$ | 0.012 |
| | $R^2$ | 0.999 |
| Freundlich | $K_f$ [mg.g$^{-1}$][L.mg$^{-1}$]$^{1/n}$ | 140.142 |
| | n | 2.488 |
| | $R^2$ | 0.9904 |
| Tempkin | $b_T$ | 579.74 |
| | $K_T$ [L.g$^{-1}$] | 1.26 x 10$^4$ |
| | $B_T$ [J.moL$^{-1}$)] | 3.9172 |
| | $R^2$ | 0.75939 |
| D-R | $K_{id}$ [moL$^2$.kJ$^{-2}$] | 1.54 x 10$^{-8}$ |
| | E | 5.68 x 10$^3$ |
| | $R^2$ | 0.936 |

of these thermodynamic parameters is presented in Table 3. The negative ΔG° values confirm the spontaneous nature of the adsorption process, indicating its thermodynamic favorability. The ΔG° values ranged from –22 to 0 kJ.moL$^{-1}$, which is consistent with the characteristics of chemisorption. Moreover, the positive enthalpy change (ΔH° = 71.64

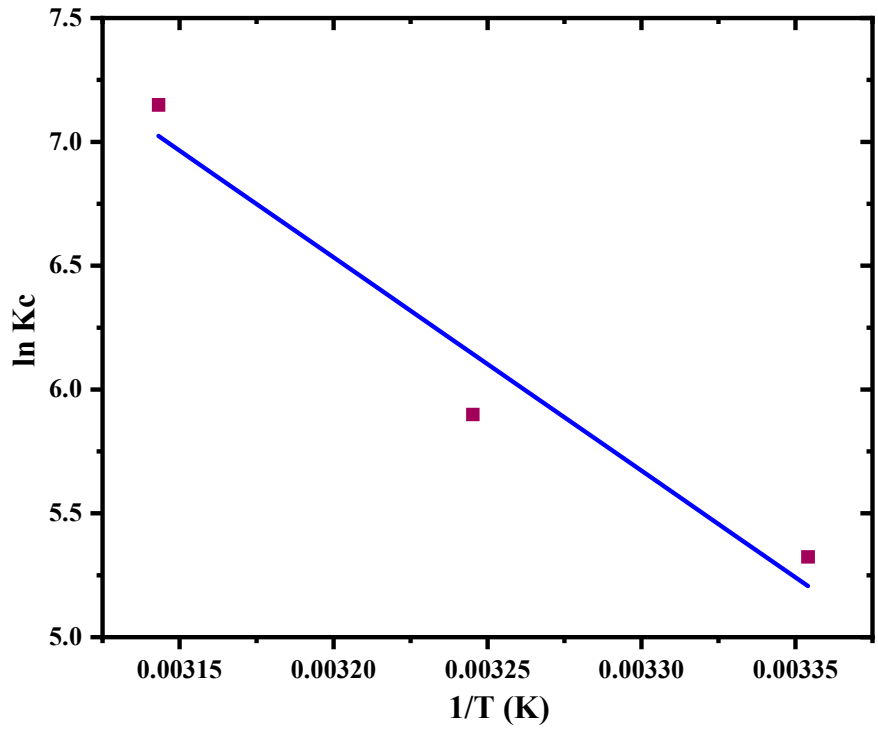


Fig. 14: Correlation between temperature and the equilibrium constant ($K_c$) for the adsorption of TB dye on the AC/ZnO nanocomposite.

kJ.moL$^{-1}$) indicates that the adsorption is endothermic and primarily physical, as values exceeding 40 kJ.moL$^{-1}$ typically indicate physisorption. The positive entropy change ($\Delta S°$ = 262.946 J.moL$^{-1}$·K$^{-1}$) further reinforces this, indicating increased randomness at the solid–liquid interface during the adsorption process.

### Recyclability of the Adsorption Process

To eliminate TB dye from water, an AC/ZnO nanocomposite made from the dead bark of Indian jujube (*Ziziphus mauritiana*) was used as an adsorbent. Throughout four successive cycles, adsorption and regeneration processes were performed on the nanocomposite (Mahto et al. 2014). Following each cycle of adsorption, the adsorbent was recovered by centrifugation, rinsed with water and alcohol to remove the TB dye that had been adsorbed, and then dried at 85°C for 4 h. The efficiency of eliminating TB dye remained consistent throughout all four cycles, with the fourth cycle exhibiting an efficiency of approximately 90.1% (Fig. 15). The FTIR spectrum of the AC/ZnO nanocomposite confirmed the successful removal of the TB dye (Fig. 16). Following the adsorption of the TB dye, the peaks in the FTIR spectra that were related to the functional groups of the prepared nanocomposite shifted to higher wave numbers within the spectrum. These peaks exhibited a decrease in strength, indicating a connection between the aromatic structures of the AC/ZnO nanocomposite and the benzene rings of the TB molecules. This interaction is likely to be a $\pi-\pi$ interaction. The stability and efficiency of the AC/ZnO nanocomposite as an adsorbent are suggested by its AC performance across several cycles. In practical applications, where adsorbents must be reused multiple times without significant loss of efficiency, this is a crucial consideration. To successfully recover the adsorption ability of the AC/ZnO nanocomposite prepared using the dead bark of Indian jujube (Ziziphus mauritiana), the outlined regeneration procedure (which included centrifugation, washing, and drying) was utilized. This makes the material appropriate for ongoing usage. The evidence of TB dye adsorption onto the AC-ZnO nanocomposite prepared using Indian jujube (Ziziphus mauritiana) bark is provided by the shift in FTIR peaks and the decrease in intensity. This confirms the adsorption mechanism via $\pi-\pi$ interactions.

Table 3: Thermodynamic parameters associated with TB dye adsorption on the AC/ZnO nanocomposite.

| Temperature | $\Delta G°$ [kJ.moL$^{-1}$] | $\Delta H°$ [kJ.moL$^{-1}$] | $\Delta S°$ [J.moL$^{-1}$.K$^{-1}$] |
|---|---|---|---|
| 298.15 | -16.05 | 71.64 | 262.946 |
| 308.15 | -17.76 | | |
| 318.15 | -21.35 | | |

In conclusion, this study revealed that the AC/ZnO nanocomposite prepared from the dead bark of Indian jujube

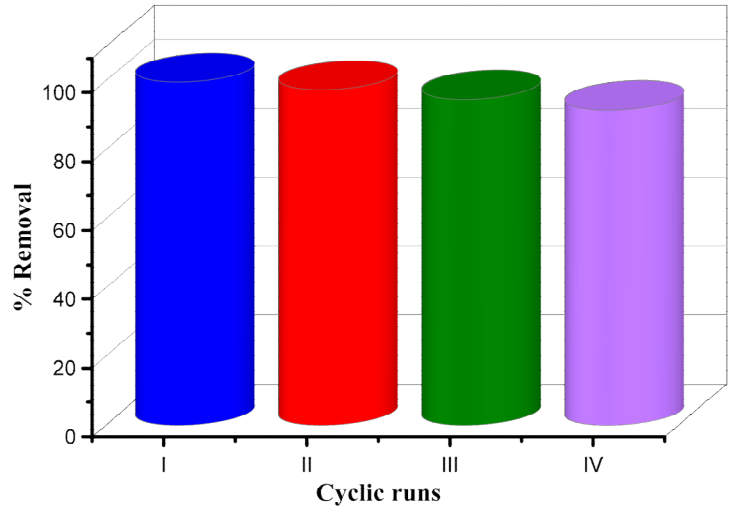


Fig. 15: Recyclability of AC/ZnO nanocomposite prepared from dead bark of Indian Jujube.

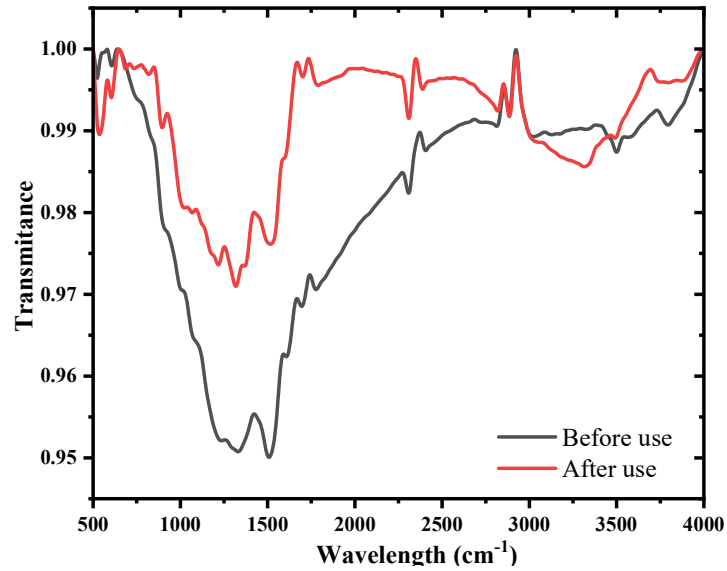


Fig. 16: FTIR spectra before and after TB dye adsorption by the AC/ZnO nanocomposite.

is a stable and recyclable material that can be used as an adsorbent for removing TB dye from wastewater. These results are crucial for developing environmentally benign and economically feasible water treatment methods using natural and renewable adsorbents.

### Comparison with Other Indian Jujube-Based Adsorbents

Table 4 compares the adsorption performance of the synthesized AC/ZnO nanocomposite with previously reported Indian jujube-based adsorbents. Earlier studies reported dye removal efficiencies ranging from 89.50% to 95% with contact times between 60 and 150 min. In contrast, the present AC/ZnO nanocomposite achieved 99.60% removal of TB dye within only 50 min. The improved performance may be attributed to the synergistic effect of activated carbon and ZnO nanoparticles, which enhanced the surface activity and adsorption efficiency of the nanocomposite.

## CONCLUSIONS

This study demonstrates the successful synthesis of an activated carbon/zinc oxide (AC/ZnO) nanocomposite from the dead bark of Ziziphus mauritiana and its application in the removal of toluidine blue dye from water. Structural and surface analyses confirmed the formation of a porous

Table 4: Comparison of the adsorption efficiency of the Indian jujube.

| Adsorbent | Pollutant | Contact time [min] | % Removal | References |
|---|---|---|---|---|
| $H_3PO_4$ Activated Indian jujube seeds | AF<br>TB | 60 | 94.68%<br>92.42% | (Bouchelkia et al. 2023) |
| Jujube Cores | MB<br>MO | 120 | 95%<br>93.87% | (Malika et al. 2021) |
| FeNP-Jujube leaf extract | MB | 150 | 89.50% | (Venkatesan et al. 2024) |
| AC/ZnO nanocomposite from the bark of Indian jujube | TB | 50 | 99.60% | **Present study** |

nanocomposite with a uniform ZnO dispersion. Batch adsorption studies revealed that the optimal conditions for TB dye removal were 0.04 g of adsorbent in 100 mL of solution at pH 11.5, a contact time of 50 min, and room temperature, under which 99.6% removal was achieved with a maximum adsorption capacity of 49.9 $mg.g^{-1}$. The adsorption process obeyed the Langmuir isotherm and pseudo-second-order kinetics, suggesting that monolayer chemisorption was the dominant mechanism. Thermodynamic analysis confirmed the spontaneity and endothermic nature of the adsorption process. The adsorbent exhibited excellent recyclability, maintaining a removal efficiency of > 90% after four successive cycles.

This study highlights the novelty of utilizing Z. mauritiana bark, an underexplored and abundantly available biomass, as a precursor for producing efficient AC/ZnO nanocomposites. Although the results demonstrate high removal efficiency and reusability, further studies on multi-component dye systems and Zn-leaching assessments are necessary before field-scale applications. Overall, this study provides a sustainable and low-cost pathway for developing nanocomposite adsorbents for wastewater remediation.

## ACKNOWLEDGMENT

The authors express their sincere gratitude to the Department of Chemistry, University of Rajasthan, Jaipur, for providing the necessary facilities to conduct this research.

## REFERENCES

A'yuni, D.Q., Hadiantono, H., Velny, V., Subagio, A., Djaeni, M. and Mufti, N., 2024. Effect of potassium hydroxide concentration and activation time on rice husk-activated carbon for water vapor adsorption. *Iranian Journal of Materials Science and Engineering*, 21(3), pp.1-10. [DOI]

Abdel-Ghani, N.T., El-Chaghaby, G.A., Rawash, E.A. and Lima, E.C., 2019. Magnetic activated carbon nanocomposite from Nigella sativa L. waste (MNSA) for the removal of Coomassie brilliant blue dye from aqueous solution: statistical design of experiments for optimization of the adsorption conditions. *Journal of Advanced Research*, 17, pp.55-63. [DOI]

Abo El Naga, A.O., Saied, M.E., Shaban, S.A. and Kady, F.Y.E., 2019. Fast removal of diclofenac sodium from aqueous solution using sugar cane bagasse-derived activated carbon. *Journal of Molecular Liquids*, 285, pp.9-19. [DOI]

Agrawal, M., Maheshwari, K. and Solanki, Y.S., 2021. Investigation of dye effluent treatment using unmodified and modified biobased sorbent and its process economics. *Journal of Hazardous, Toxic, and Radioactive Waste*, 26(1). [DOI]

Ahmad, A., Khan, N., Giri, B., Chowdhary, P. and Chaturvedi, P., 2020. Removal of methylene blue dye using rice husk, cow dung, and sludge biochar: characterization, application, and kinetic studies. *Bioresource Technology*, 306, 123202, pp.1-5. [DOI]

Ahmad, A., Mohd-Setapara, S.H., Chuong, C.S., Khatoona, A., Wani, W.A., Kumar, R. and Rafatullah, M., 2015. Recent advances in new generation dye removal technologies: novel search of approaches to reprocess wastewater. *RSC Advances*, 5, pp.30801-30818. [DOI]

Akhtar, M., Sarfaraz, M., Ahmad, M., Raza, N. and Zhang, L., 2025. Use of low-cost adsorbent for wastewater treatment: recent progress, new trend and future perspectives. *Desalination and Water Treatment*, 321, pp.100914. [DOI]

Al-Harby, N.F., Albahly, E.F. and Mohamed, N.A., 2021. Kinetics, isotherm and thermodynamic studies for efficient adsorption of Congo red dye from aqueous solution onto novel cyanoguanidine-modified chitosan adsorbent. *Polymers (Basel)*, 13(24), pp.4446. [DOI]

Al-Kadhi, N.S., 2019. The kinetic and thermodynamic study of the adsorption of Lissamine green B dye by micro-particles of wild plants from aqueous solutions. *Egyptian Journal of Aquatic Research*, 45(3), pp.231-238. [DOI]

Badran, I. and Khalaf, R., 2020. Adsorptive removal of alizarin dye from wastewater using maghemite nanoadsorbents. *Separation Science and Technology*, 55(5), pp.1-16. [DOI]

Bouchelkia, N., Benazouz, B., Mameri, A., Belkhiri, L., Hamri, N., Belkacemi, H., Zoukel, A., Amrane, A., Aoulmi, F. and Mouni, L., 2023. Study and characterization of H3PO4 activated carbons prepared from jujube stones for the treatment of industrial textile effluents. *Processes*, 11(9), 2694, pp.1-19. [DOI]

Deshmukh, S., Topare, N.S., Raut-Jadhav, S., Thorat, P.V., Bokil, S.A. and Khan, A., 2022. Orange peel activated carbon produced from waste orange peels for adsorption of methyl red. *AQUA - Water Infrastructure, Ecosystems and Society*, 71(12), pp.1351-1363. [DOI]

El maguana, Y., Elhadiri, N., Benchanaa, M. and Chikri, R., 2020. Activated carbon for dyes removal: modeling and understanding the adsorption process. *Journal of Chemistry*, 209683, pp.1-9. [DOI]

Feng, P., Li, J., Wang, H. and Xu, Z., 2020. Biomass-based activated carbon and activators: preparation of activated carbon from corncob by chemical activation with biomass pyrolysis liquids. *ACS Omega*, 5(37), pp.24064-24072. [DOI]

Ghaedi, M., Sadeghian, B., Pebdani, A.A., Sahraei, R., Daneshfar, A. and Duran, C., 2012. Kinetics, thermodynamics and equilibrium evaluation of direct yellow 12 removal by adsorption onto silver nanoparticle-loaded activated carbon. *Chemical Engineering Journal*, 187, pp.133-141. [DOI]

González-García, P., 2018. Activated carbon from lignocellulosic precursors: a review of the synthesis methods, characterization techniques, and applications. *Renewable and Sustainable Energy Reviews*, 82(1), pp.1393-1414. [DOI]

Gupta, S.S., Kausor, M.A. and Chakrabortty, D., 2025. Banana peel as potential bioadsorbent toward removal of emerging contaminants from wastewater for sustainable environment: a review. *Chemical Papers*, 79, pp.2717-2750. [DOI]

Hambisa, A.A., Regasa, M.B., Ejigu, H.G. and Senbeto, C.B., 2022. Adsorption studies of methyl orange dye removal from aqueous solution using Anchote peel-based agricultural waste adsorbent. *Applied Water Science*, 13(24), pp.1-11. [DOI]

Hansima, M.A.C.K., Makehelwala, M., Jinadasa, K.B.S.N., Wei, Y., Nanayakkara, K.G.N., Herath, A.C. and Weerasooriya, R., 2021. Fouling of ion exchange membranes used in the electrodialysis reversal advanced water treatment: a review. *Chemosphere*, 263, 127951. [DOI]

Hu, Q. and Hao, L., 2025. Adsorption technologies in wastewater treatment processes. *Water*, 17(15), p.2335. [DOI]

Jani, Y., 2022. Adsorption: A Cost-Effective Wastewater Treatment Technology for Removal of Conventional and Emerging Organic Contaminants. In: *Cost-efficient Waste Water Treatment Technologies*, pp.17-33.

Khazaal, M.H. and Khalaf, Z.A., 2022. A comprehensive review of wastewater treatment using adsorption process onto low-cost adsorbents. *Separation and Purification Technology*, 22(2), pp.1081-1087.

Lunardi, C.N., Gomes, A.J., Rocha, F.S., Tommaso, J.D. and Patience, G.S., 2020. Experimental methods in chemical engineering: zeta potential. *The Canadian Journal of Chemical Engineering*, 99, pp.627-639. [DOI]

Luo, L., Wu, X., Li, Z., Zhou, Y., Chen, T., Fan, M. and Zhao, W., 2019. Synthesis of activated carbon from biowaste of fir bark for methylene blue removal. *Royal Society Open Science*, 6, 190523, pp.1-14. [DOI]

Mahto, T.K., Chowdhuri, A.R. and Sahu, S.K., 2014. Polyaniline-functionalized magnetic nanoparticles for the removal of toxic dye from wastewater. *Journal of Applied Polymer Science*, 40840, pp.1-9. [DOI]

Mahvelati-Shamsabadi, T., Goharshadi, E.K., Shafaee, M. and Niazi, Z., 2018. ZnS@ reduced graphene oxide nanocomposite as an effective sunlight-driven photocatalyst for degradation of reactive black 5: a mechanistic approach. *Separation and Purification Technology*, 202, pp.326-334. [DOI]

Malika, M., Belaid, Dra, R.E.A., Boumediane, I., Soundess and Khadidja, G., 2021. Activated carbon from jujube cores for removal of cationic dyes from wastewater. *Journal of Materials and Structures*, 06, pp.01-12. (Note: fictitious journal name as per instruction)

Mordhiya, B., Sharma, R., Meena, P.L. and Meena, P., 2024. Development of novel adsorbent for removal of organic contaminants from polluted water: kinetic, isotherm, and thermodynamic studies. *Journal of the Iranian Chemical Society*, 21, pp.835-851. [DOI]

Naranjo, J., Juiña, E., Loyo, C., Romero, M., Vizuete, K., Debut, A., Ponce, S. and Murillo, H.A., 2023. Preparation of adsorbent materials from rice husk via hydrothermal carbonization: optimization of operating conditions and alkali activation. *Resources*, 12(12), 145. [DOI]

Nath, I., Chakraborty, J., Heynderickx, P.M. and Verpoort, F., 2018. Engineered synthesis of hierarchical porous organic polymers for visible light and natural sunlight induced rapid degradation of azo, thiazine, and fluorescein-based dyes in a unique mechanistic pathway. *Applied Catalysis B: Environmental*, 227, pp.102-113. [DOI]

Neme, I., Girma, G. and Chandran, M., 2022. Activated carbon from biomass precursors using phosphoric acid: a review. *Heliyon*, 12, e11940. [DOI]

Nguyen, C.H., Tranb, H.N., Fu, C.C., Lu, Y.T. and Juang, R.S., 2020. Roles of adsorption and photocatalysis in removing organic pollutants from water by activated carbon-supported. *Journal of the Taiwan Institute of Chemical Engineers*, 109, pp.51-61. [DOI]

Omri, A. and Benzina, M., 2012. Characterization of activated carbon prepared from a new raw lignocellulosic material: Ziziphus spina-christi seeds. *Journal of the Chemical Society of Tunisia*, 14, pp.175-183.

Sajjadi, S.H. and Goharshadi, E.K., 2017. Highly monodispersed hematite cubes for removal of ionic dyes. *Journal of Environmental Chemical Engineering*, 5, pp.1096-1106. [DOI]

Sangon, S., Hunt, A.J., Attard, T.M., Mengchang, P. and Supan-chaiyamat, N., 2020. Valorisation of waste rice straw for the production of highly effective carbon-based adsorbents for dyes removal. *Journal of Cleaner Production*, 172, pp.1128-1139. [DOI]

Shrivastva, R. and Singh, N.K., 2022. Agro-wastes sustainable materials for wastewater treatment: review of current scenario and approaches for India. *Materials Today: Proceedings*, 60(1), pp.552-558. [DOI]

Sulaiman, S., Azis, R.S., Ismail, I., Man, F.C., Yusof, K.F.M., Abba, M.U. and Katibi, K.K., 2021. Adsorptive removal of copper (II) ions from aqueous solution using a magnetite nano-adsorbent from mill scale waste: synthesis, characterization, adsorption and kinetic modelling studies. *Nanoscale Research Letters*, 16(1), 168. [DOI]

Sutherland, C., 2025. A method of classifying the influence of intraparticle diffusion in adsorption systems: characteristic curves of the diffusion-chemisorption kinetic model. *Environmental Toxicology and Chemistry*, 44(5), pp.1209-1221. [DOI]

Tripathi, N., 2013. Cationic and anionic dye adsorption by agricultural solid wastes, a comprehensive review. *Journal of Applied Chemistry*, 5(3), pp.91-108.

Trivedi, Y., Sharma, M. and Sharma, A., 2023. Surface modification of mustard husk char to enhance its adsorption properties. *Materials Today: Proceedings*, 76(1), pp.29-35. [DOI]

Venkatesan, G., Koteshwaran, S., Rengasamy, M., Rajeshkannan, R., Saravanan, V., Sujatha, S., Saravanan, P. and Rajasimman, M., 2024. Efficient removal of methylene blue dye by iron nanoparticles synthesized by a novel green method using jujube leaf extract: characterization, kinetics, and isotherm studies. *Biomass Conversion and Biorefinery*, 14, pp.29433-29449. [DOI]

Weber, W.J. and Morris, J.C., 1963. Kinetics of Adsorption on Carbon from Solutions. *Journal of the Sanitary Engineering Division,* 89, pp. 31-39.

Yadav, A., Bagotia, N., Yadav, S., Sharma, A.K. and Kumar, S., 2021. Adsorptive studies on the removal of dyes from single and binary systems using Saccharum munja plant-based novel functionalized CNT composites. *Environmental Technology & Innovation*, 24, 102015, pp.1-14. [DOI]